JOURNAL OF AIRCRAFT
Vol. 47, No. 4, July–August 2010

Real Time Morphing Wing Optimization Validation Using Wind-Tunnel Tests

Andrei V. Popov,* Lucian T. Grigorie,† and Ruxandra Botez‡
École de Technologie Supérieure, Montréal, Québec H3C 1K3, Canada
and
Mahmoud Mamou§ and Youssef Mébarki¶
National Research Council, Ottawa, Ontario K1A 0R6, Canada

DOI: 10.2514/1.47431

In this paper, wind-tunnel results of a real time optimization of a morphing wing in the wind tunnel for delaying the transition toward the trailing edge are presented. A morphing rectangular finite aspect ratio wing, having a wind tunnel experimental airfoil reference airfoil cross section, was considered, with its upper surface made of a flexible composite material and instrumented with Kulite pressure sensors and two smart memory alloys actuators. Several wind-tunnel test runs for various Mach numbers, angles of attack, and Reynolds numbers were performed in the 6′ × 9′ wind tunnel at the Institute for Aerospace Research at the National Research Council Canada. Unsteady pressure signals were recorded and used as feedback in real time control while the morphing wing was requested to reproduce various optimized airfoils by changing automatically the two actuators' strokes. This paper shows the optimization method implemented into the control software code that allows the morphing wing to adjust its shape to an optimum configuration under the wind-tunnel airflow conditions.

Nomenclature

b	=	span of wing model, m
c	=	chord of wing airfoil, m
C_D	=	drag coefficient
C_L	=	lift coefficient
C_p	=	pressure coefficient
M	=	Mach number
N	=	natural logarithm of rapport between amplified perturbation and initial perturbation in laminar flow
Re	=	Reynolds number
x_{tr}	=	transition position, m
α	=	angle of attack of the wing, deg

I. Introduction

THE Consortium for Research and Innovation in Aerospace in Quebec 7.1 project was a collaborative project between the teams from École de technologie superieure (ETS), École Polytechnique, the Institute for Aerospace Research, National Research Canada (IAR-NRC), Bombardier Aerospace, and Thales Avionics. In this project, the laminar flow past aerodynamically morphing wing was improved to obtain important drag reductions.

This collaboration called for both aerodynamic modeling as well as conceptual demonstration of the morphing principle on real models placed inside the wind tunnel. Drag reduction on a wing could be achieved by modifications of the airfoil shape, which had an effect in the laminar-to-turbulent flow transition point position. The main objective of this concept was to promote large laminar regions on the wing surface by moving the transition point toward the trailing edge of the airfoil wing, thus reducing drag over an operating range of flow conditions characterized by Mach numbers, airspeeds, and angles of attack [1].

To modify the laminar flow around a wing airfoil, it was necessary to change the airfoil shape; therefore, one of the methods for airfoil changes was developed at Kentucky University, which consisted of deflecting the wing upper surface using adaptive actuators [2–7].

It was shown that the actuators activated oscillatory motions of a certain frequency to the boundary-layer flow over the upper surface. These actuators were made of piezo-electric materials that changed their shapes when connected to an electrical current differential voltage. The wind-tunnel tests showed that the displacement of the transition point to the trailing edge resulted in the drag decrease and in the lift increase [3].

Another method for changing the airfoil shape involved the use of a bump, which was inflated with air. This method was conceived by researchers at Stuttgart University [8,9]. In this method, the airfoil geometry was modified to decrease the negative effects of shock-waves in transonic flow. The results obtained by the airfoil optimization showed a 70% decrease in the wave drag and a 15% decrease in the wing total drag.

At the German Aerospace Research Center (DLR), researchers simulated the changes of the airfoil shape using an inflated bump [10,11]. The results obtained showed a 10% drag reduction for Mach numbers between 0.72 and 0.77. A basic theory was developed for changing the airfoil shape in transonic flow.

Another method for changing the airfoil shape was studied by the aerospace company Embraer [12–15]. In this case, the leading and trailing edges changed their shapes by curving the camber line. The results obtained by Embraer were promising as they showed a reduction in drag value by up to 24%.

A 1991 study conducted at NASA Langley Research Center laboratory evaluated the application of the hybrid laminar flow control on subsonic aircrafts and bimotor aircraft transporters [16]. The study was realized by using the flight optimizing system as well as a computational fluid dynamics (CFD) code. The researchers studied the laminar flow over the upper surface of the wing, and over the

Received 29 September 2009; revision received 4 December 2009; accepted for publication 5 December 2009.

*Ph.D. Student, Laboratory of Research in Active Controls, Avionics and AeroServoElasticity, 1100 Notre-Dame West Street. Member AIAA.

†Postdoctoral Fellowship, Laboratory of Research in Active Controls, Avionics and AeroServoElasticity, 1100 Notre-Dame West Street. Member AIAA.

‡Professor, Laboratory of Research in Active Controls, Avionics and AeroServoElasticity, 1100 Notre-Dame West Street. Member AIAA.

§Senior Research Officer, Aerodynamics Laboratory, Montreal Road, Uplands Building U66. Member AIAA.

¶Associate Research Officer, Aerodynamics Laboratory, Montreal Road, Uplands Building U66. Member AIAA.

vertical and horizontal stabilizers. They also studied the advantages of the laminar flow over the nacelles.

The chordwise air collection method was designed in 1984. In fact, laminar flow control over the upper surface of the wing was realized by the boundary-layer suction, thereby moving the transition position at 85% of the chord [17].

A numerical algorithm was developed for optimizing the suction distribution, by maintaining the transition at a desired location (chord %) and maintaining the energy spent at a minimum [18]. Three steps were considered: 1) boundary-layer computation, 2) transition prediction, and 3) optimization of the suction distribution while maintaining the transition location at a certain desired percentage of the chord. In the third step, the gradient method was used. Optimized wings were conceived by reducing the kinetic energy of the perturbation and drag values, while the lift and pitch moment coefficients were maintained at desired values [19].

At DLR, the DoAL3 airfoil was designed for aircraft wings at moderate Mach numbers $M = 0.45$–0.6, and at Reynolds numbers up to $Re = 14 \times 10^6$. Transition measurements were performed in the Brunswick Wind Tunnel at Mach number of 0.48. The effects of Reynolds number and the thermal transfer on the laminar flow separately were studied, and the numerical results were validated by experiments.

A controller was developed at Southampton University with the aim of maintaining the desired turbulence level over a flat plate equipped with a suction porous panel. The pressure fluctuations were measured with microphones at the boundary layer over the flat plate, and the signal was conditioned and filtered to remove the background noise of the wind-tunnel fan. Then, the turbulence level was estimated by computing the rms pressure signal. The controller used the error between the rms values of the measured pressures and the desired rms values at the spots where the microphones were installed, thus maintaining the transition on the specified area over the flat plate [20].

Three devices were capable of modifying wing structure on a test bed aircraft [21]. The first device was the Hyper-Elliptic Cambered Span (HECS) wing mechanism, used to increase loiter time. During cruise, induced drag accounted for 50% of the total aircraft drag. Compared with a planar elliptic wing of the same span, the HECS wing provided a lift-to-drag ratio (L/D) increase of as much as 15%, with a 10% increase in surface area. The second device was the oblique joint mechanism, located at the root of a standard planar elliptical airfoil, and capable of independently rotating each wing on an aircraft through variations of dihedral, sweep, and incidence angles, by use of three sequential motors per wing that can be operated independently. The third device employed a Stewart platform concept as a constrained version of the six degree-of-freedom (DOF) mechanism commonly used, with a central pivot preventing translational motion and allowing rotation about the center of the top and bottom plate using three Haydon Switch and Instrument $\frac{1}{2}$ stroke linear actuators. Compliant skin materials were also discussed.

A strain energy model took into account the actuation cost of a morphing airfoil, where a multi-objective optimization found tradeoff solutions between low-energy/high-drag and high-energy/low-drag morphing airfoils [22]. The aerodynamic work term was added to the strain energy model to compute the total energy required for the airfoil shape change. The effect of the morphing airfoil's relative stiffness on the multi-objective solutions was presented.

Stabilators were used for various applications such as primary and secondary flight control, buffet-load alleviation, flutter testing, active flow reattachment, and vortex generation. However, most of the adaptive aerostructures' applications were found in unmanned aerial vehicles (UAVs), missiles, and munitions [23].

Closed-loop control of the morphing planform (wing-shape control) and simultaneously enforced prescribed closed-loop aircraft dynamics (flight control) were modeled [24]. The N-MAS wing designed by NextGen Aeronautics was considered. The flight control law actively used the leading-edge morphing wing sweep angle as an actuator to assist in manoeuvres while guaranteeing aircraft stability. An aircraft model (morphing wing, aircraft body, and control surface locations) was developed using CAD drawings, mass and geometry specifications, and NACA airfoil designations. The Simulink model included variable (center of gravity) and DATCOM-derived aerodynamic coefficients as a function of the wing configuration and angle of attack. The morph between the two modes of loiter and dash was modeled by a first-order transfer function, and hence the morph rate was governed by the transfer function time constant.

The empirical structural weights for various wing geometries were obtained by implementing two finite element-based structural optimization methods: 1) an aggregate, and 2) a simultaneous analysis [25]. These methods were applied on a morphing wing with 2 DOF: the wing sweep and the root chord length. Two linear actuators were used: one positioned along and parallel to the forward spar and the other one positioned along and parallel to the wing root chord. These geometrical variations produced four configurations with changes in area, aspect ratio, and sweep: the high-lift configuration for the largest area and minimal sweep angle, the loiter configuration for the maximum aspect ratio and minimum sweep angle, the dash/cruise configuration for the maximum sweep and minimal area, and the manoeuvre configuration for the maximum area at the maximum sweep.

Northrop Grumman Corporation has built and tested two 16% scale wind-tunnel models (conventional and smart) of a fighter aircraft under the Defense Advanced Research Projects Agency (DARPA)/Air Force Research Laboratory (AFRL)/NASA Smart Wing Phase I project [26]. Hinge-less, contoured trailing-edge (TE) control surfaces with embedded shape memory alloy (SMA) wires and spanwise wing twists effected by SMA torque tube mechanisms were compared with the conventional hinged control surfaces. Benefits were expressed in terms of increased pitching and rolling moments, and improved pressure distributions. Successful results were expressed in terms of: 1) 5 deg of spanwise twist and an 8–12% increase in rolling moment using a single SMA torque tube, 2) 12 deg of deflection and 10% increase in rolling moment, and 3) demonstration of optical techniques for span twist and deflected shape measurements.

A symmetric wing structure was created with two tapered graphite/epoxy composite plates and a steel body. Four pairs of SMA wires were attached to the wings' bottom surfaces in the chordwise direction. Lift and drag forces were measured at various angles of attack. Dynamic vibration signals were measured by Fiber Bragg Grating sensors at the wing root and were used to monitor aeroelastic unstable flutter phenomena at various angles of attack [27].

A wing structure composed of an optimized internal layout of cables and struts was able to change its shape. Cables were used as actuators, and struts provided rigidity to the wing. In addition to achieving continuous morphing by changing cable lengths, this structure had the advantages of being lightweight and having a distributed actuation. Topology optimization was used to optimally place cables and struts in a bay or in a wing section. The nondominated sorting genetic algorithm II (NSGA II) was used for modeling the NASA HECS and the NextGen TSCh wings [28].

An integrated multidisciplinary optimization procedure for morphing wing optimization was mainly based on off-the-shelf analysis codes. It allowed the computation of the minimum structural weight of morphing wings (for which swept angle and aspect ratio change). This optimization was performed with a general-purpose optimization code, called Optimus, distributed by Noesis Solutions. For aeroelasticity studies, MSC/Nastran and ALIS (for steady and unsteady linear aerodynamics) codes were used. Two approaches were presented: sequential and fully integrated. An LMS Virtual Lab Morphing tool was also used [29].

Wings roll performances were achieved by use of articulated conformal control surfaces. Analysis results were compared with experimental results obtained for a 16% scale model of a fighter wing equipped with embedded smart materials used to deform a control surface. The control surface design was found suitable for low-rate applications such as takeoff and landing configurations [30].

Lockheed Martin built an unmanned combat air vehicle for morphing A/C studies. Its configuration had two folds that allowed the radical morphing of the span and wetted area. The multirole aerodynamic performance was defined by a combination of cruise/loiter efficiency and dash/penetration capability in a single vehicle,

and by significantly increasing the mission performance with respect to the conventional platforms. Both inboard and outboard flaps were required for manoeuvring and pitch/yaw stability [31]. An articulated large-scale half-span wind-tunnel model-validated morphing system operation under realistic flight loads was realized [32].

Four application fields of the SMA's technology on an aircraft have been investigated: vibration/acoustic control, shape control, multifunctional smart structures, and morphing structures. Tail-buffet suppression, flutter damping, engine-vibration control, smart wing, smart skin, adaptive micro air vehicle, vortex wake control, and biology-inspired aircraft were reviewed. The best technology application would be a reconfigurable configuration for which performances would be adjusted and optimized under varying conditions [33].

The MFX-1, created under a DARPA sponsored program called Next Generation Morphing A/C Structures (N-MAS) and realized by NextGen Aeronautics, had a 9.3 ft wing span, a length of 6.8 ft, *V*-tails, nonretractable landing gear with a steerable nose wheel, three onboard cameras with one download link, and a GPS system. It was powered by a single jet engine with 45 lb of maximum thrust. Other key features included independently activated ailerons, flaps, rudders, GPS, microelectric mechanical system gyros and accelerometers as flight control system sensors, altitude telemetry, airspeed, GPA headings, battery conditions, maximum flight time of 20 min, and a parachute flight termination/recovery system. The primary purposes of these tests were to 1) demonstrate in-flight operation at subscale, and stability and control of the MFX-1, and 2) test flight-test procedures including communications and pilot skills for N-MAS aircraft.

During the first test a fixed wing was flown, which provided good training for the flight-test crew. During the second test, performed on the morphing wing, multiple checks of the morphing wing actuation and power systems were performed before flight to reduce the overall test risk [34]. The flight took place at altitudes between 400 and 600 ft, and at speeds between 100 and 120 kt. The remote pilot had no cues except aircraft views from the ground. Onboard recorded data included GPS location and altitude, and three video cameras, mounted on the twin tails of the aircraft and in its nose, provided flight pictures to be downloaded after landing. The wing area changed 40%, the wing span changed 30%, and the wing sweep varied from 15 to 35 deg to successfully morph during flight, of less than 15 sec. During Phase II of the N-MAS program, a 200 lb, autonomous, twin-jet morphing UAV had a larger and improved wing design that rapidly morphed during manoeuvres required for agile hunter–killer operations.

The probabilistic modeling of actuator failure and stochastic robust control provided a novel and flexible means of failure compensation for a morphing tailless, delta-wing fighter aircraft operating arrays of large numbers of actuation devices [35]. Lateral equations of motion were linearized at Mach number $M = 0.6$ and altitude $H = 15,000$ ft. The equilibrium trim angle of attack was approximately 4.4 deg. Control moments required at the trim condition were generated by conventional hinged surface actuators. The shape-change effectors/device arrays were used to stabilize and manoeuvre the vehicle at the trim condition. Among the four distributed arrays of shape-change devices on each wing, three are situated on the upper surface and one is on the lower wing surface. There were a total of 156 devices, 78 on each wing [36].

NextGen developed an in-plane morphing geometry concept. Flexible elastomeric skins with out-of-plane stiffeners accommodated the wing motion while transmitting air pressure loads to the wing substructure. Wind-tunnel testing of a full-scale wing for a 2400 lb vehicle and flight testing of a subscale UAV were performed. The following issues were identified: 1) the need to address multiple geometries and flight envelopes to account for morphing shape changes, and 2) the in-plane wing flexibility resulting from its mechanism restraint by linear actuators. Another half-span wind-tunnel model was tested in the NASA Transonic Dynamics Tunnel for aeroelasticity studies [35].

The miniature trailing edge effector was a small TE device located at 1–5% chord, deflected vertically into the flow. A stable separation region ahead of the flap and a pair of counter-rotating vortices aft were realized. Aerodynamic analysis results provided a database for the development of the aerodynamic wind-tunnel test model. The aeroservoelastic test model successfully proved an active flutter suppression concept for an UAV [37].

An aeroelastic numerical code took into account the morphing energy coupled with a 3-D beam finite elements model in a corotational framework to a lifting line aerodynamic code. The morphing energy was calculated by the sum of actuation moments, applied at the beam nodes, multiplied by the required angular rotations of the beam elements. The code results were validated with Nastran Aeroelasticity Module. This code was tested for a sweep morphing manoeuvre, and it was demonstrated that sweep morphing improved aircraft aerodynamic performances such as the lift-to-drag ratio (L/D) values.

The flight-test results of a mission adaptive compliant wing (MAC-Wing) variable geometry trailing-edge flap with a natural laminar flow airfoil have been described. The MAC-Wing technology provided lightweight, low-power, variable geometry reshaping of the upper and lower flap surface with no discontinuities. The airfoil-flap system was optimized to maximize the laminar boundary-layer extent over a broad lift coefficient range for endurance aircraft applications. The expanded laminar bucket capability allowed the endurance aircraft to extend their range, by 15% or more, by optimizing the lift-to-drag ratio (L/D) throughout the mission. The wing was tested at full-scale dynamic pressure, Mach number, and reduced-scale Reynolds numbers on Scaled Composites' Knight Aircraft. Laminar flow regime occurred up to 60% chord of the wing during tests. Significant fuel and weight savings as well as high-control authority were verified by tests and analyses. Fifteen Dantec Dynamics hot film sensors measured the boundary-layer transition position [38].

The MORPHEUS wind-tunnel model of a morphing air vehicle was designed for the following five purposes: quasi-steady aerodynamic modeling of an aircraft with large planform changes, optimization studies to achieve efficient flight configurations, transient aerodynamic modeling of high-rate planform changes, planform manoeuvring evaluations as control effectors, and gimballed flight control simulation of a morphing aircraft [39].

In the air-to-air fighter (AAF) model consisting of a propulsion subsystem and an airframe subsystem-aerodynamics (AFS-A), the morphing wing was allowed to change its sweep, length, root, and tip chord lengths within set constraints for its AAF mission of 19 flight segments. Using minimum fuel burned as an objective, the most efficient wing configuration and the overall aircraft system operation were achieved for each segment of the mission [40].

A DARPA-sponsored wind-tunnel test model of a Lockheed Martin morphing concept was designed and tested. The wind-tunnel model incorporated the key features representative of a full-scale vehicle model: out-of-plane morphing through a coordinated actuation system integrated with seamless skins and a composite support structure that encompassed the actuator system along the wing fold hinge lines, structural layout and materials featured in the full-scale vehicle design, and a first-time thermopolymer actuator integral to a leading-edge device for smooth contour between the inner wing and fuselage when fully morphed. The model was instrumented with strain gauges, accelerometers, and pressure transducers; data were acquired and correlated with aircraft design and analysis methods [41].

The airborne modification of an aircraft wing airfoil shape could be realized continuously to maintain laminar flow over the wing surface as flight conditions changed. To achieve such a full operating concept, a closed-loop control system concept was developed to control the flow fluctuations over the wing surface with the deformation mechanisms (actuators) [42].

The wing model had a rectangular plan form of aspect ratio of 2 and was equipped with a flexible upper surface skin on which shape memory alloys actuators were installed [43,44]. Two shape memory alloys (SMA) actuators created the displacement of the two control points on the flexible skin to realize the optimized airfoil shapes [45].

As reference airfoil, the laminar airfoil wind tunnel experimental airfoil (WTEA) was used because it was already optimized for

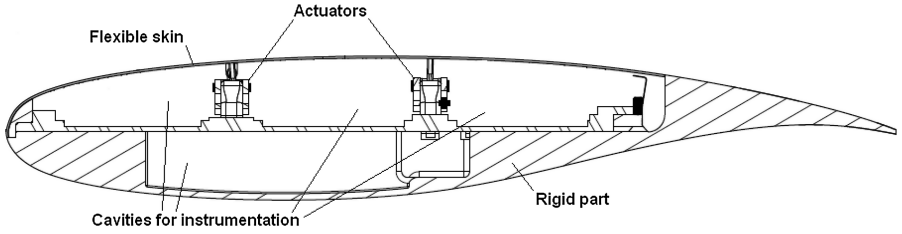

Fig. 1 Cross section of the morphing wing model.

laminar flow in the transonic regime. Its aerodynamic performance was investigated at IAR-NRC in [46,47]. The optimized airfoils were previously calculated by modifying the reference airfoil for each airflow condition as combinations of angles of attack and Mach numbers such that the transition point position was found to be the nearest as possible to the airfoil trailing edge [45]. Several optimized airfoils were found for the airflow case combinations of Mach numbers and angles of attack. The optimized airfoils configurations were stored in the computer memory by means of a database and were selected as needed by the operator or computer to be realized by the morphing wing [48]. But this strategy relied on the previously calculated aerodynamic characteristics of the airfoils, which usually were determined by use of CFD codes and optimization algorithms.

The idea presented in this paper is to implement the same optimization algorithm into the computer controller that will search the optimal configuration with the real system, in real time and for real aerodynamic airflow conditions. The basic idea of optimization control is to bypass the necessity of a previously calculated optimized airfoils database, and to generate in real time the optimized airfoil for the exact conditions of the wind flow. For such a task it was necessary to develop a subroutine that optimized the airfoil shape in the same way in which the optimized airfoils database was generated. The method of optimization used in this case was a mixed method between the gradient ascent or hill climbing method and the simulated annealing, which is a metaheuristic search method.

The hill climbing method is a local search optimization algorithm. It considers a random poor solution, which improves slowly by iterations. When the solution cannot be further improved, it becomes the final solution and the algorithm ends. In our case, the searching domain is defined by the actuators' displacements as variables, and the cost function needed to be maximized is the transition point position x_{tr}. Normally the function is defined analytically and the maximum is searched along the lines with the maximum local derivatives or gradients. Although hill climbing would be very fast and simple to program, the solution found is not guaranteed to be the global maximum of the entire search domain**. Other local search algorithms such as stochastic hill climbing, random walks, and simulated annealing would overcome this problem. The characteristic of these methods is that the algorithm searches random solutions within the search domain to cover all the possible local maxima and to find the global maximum††.

The reason why a mixed method was needed was because the cost function for such a complex problem (minimize the C_D, maximize the C_L/C_D, or maximize the transition point position x_{tr} for a morphing wing) was not defined analytically and the implementation of the gradient ascent method was not suitable. Also, due to time cost (very long time response of the SMA actuators due to heating but especially cooling time), a purely probabilistic metaheuristic search algorithm such as stochastic hill climbing, random walks, or simulated annealing was not suitable either.

The idea of the present algorithm was the mixture of the hill climbing method with the random walks or simulated annealing and the search within the defined domain nine points, one being the center of a circle and the other eight being situated on the circle with a predefined radius. When the maximum is found within the nine points, the algorithm reset the next searching step by iterating with eight points situated on smaller circles until the global maximum is found. This mixed method was found to be the fastest, that is, it considered the least number of points evaluated for converging to the transition point position x_{tr} maximum.

II. Experimental Setup Description

A. Mechanical and Electrical Control System

The concept of this morphing wing consisted of a rectangular wing model (chord $c = 0.5$ m and span $b = 2.1$ m) incorporating two parts. One fixed part was built in aluminum by the IAR-NRC team and sustained the resistance forces acting during wind-tunnel tests. The other part consisted of a flexible skin installed on a metallic structure on the wing upper surface and was designed and manufactured at ETS (Fig. 1). The flexible skin was required to change its shape through two action points to realize the optimized airfoil for the airflow conditions in which tests were performed.

The actuators were composed of two oblique cams sliding rods spanwise positioned that converted the horizontal movement along the span in vertical motion perpendicular to the chord (Fig. 2). The position of each actuator was given by the mechanical equilibrium between the Ni-Ti alloy SMA wires that pulled the sliding rod in one direction and the gas springs that pulled the sliding rod in the reverse direction. The gas springs role was to counteract the pulling effect of aerodynamic forces acting in wind tunnel over the flexible skin when the SMAs were inactive. Each sliding rod was actuated by means of three parallel SMA wires connected to a current controllable power supply, which was the equivalent of six wires acting together. The pulling action of the gas spring retracted the flexible skin in the undeformed-reference airfoil position, and the pulling action of the SMA wires deployed the actuators in the load mode, that is, morphed airfoil in the optimized airfoil position (see Fig. 2). The gas springs used for these tests were charged with an initial load of 225 lbf (1000 N) and had a characteristic rigidity of 16.8 lbf/in (2.96 N/mm).

The mechanical SMA actuators system was controlled electrically through an open-loop control system. The architecture of the wing model open-loop control system, SMA actuators, and controller is shown in Fig. 3. The two SMA actuators had six wires each, which were supplied with power by the two Amrel SPS series power supplies, controlled through analog signals by the NI-DAQ USB 6229 data acquisition card. The NI-DAQ was connected to a laptop through a universal serial bus connection. A control program was implemented in Simulink that provided to the power supplies the

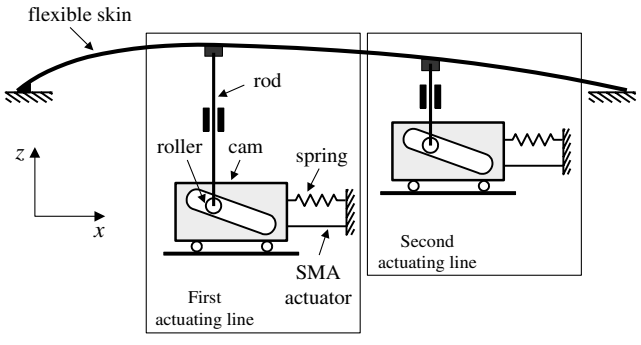

Fig. 2 Schematics of the flexible skin mechanical actuation.

**Data about hill climbing available online at http://en.wikipedia.org/wiki/Hill_climbing [retrieved 26 Nov. 2009].

††Data about simulated annealing available online at http://en.wikipedia.org/wiki/Simulated_annealing [retrieved 26 Nov. 2009].

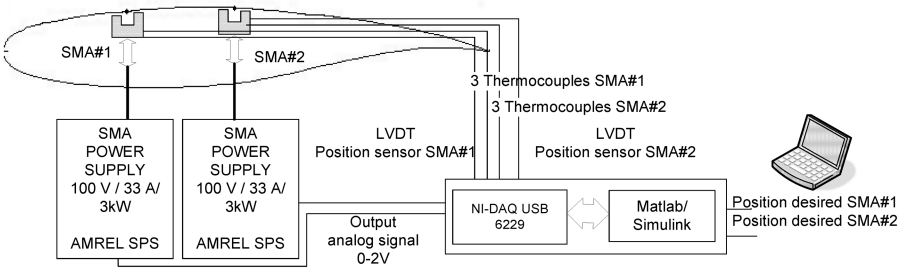

Fig. 3 Architecture of the morphing wing model control system.

needed SMA current values through an analog signal as shown in Fig. 3. The control signal of 2 V corresponded to an SMA supplied current of 33 A. The Simulink control program used as feedback three temperature signals coming from three thermocouples installed on each wire of the SMA actuator, and a position signal from a linear variable differential transducer connected to the oblique cam sliding rod of each actuator. The temperature signals served in the overheat protection system that disconnected the current supply to the SMA in case of wire temperature passed over the set limit of 120°C. The position signals served as feedback for the actuator desired position control. The oblique cam sliding rod had a horizontal versus vertical ratio 3:1; hence, the maximum horizontal displacement of the sliding rod by 24 mm was converted into a maximum vertical displacement of the actuator and implicit of the flexible skin by 8 mm.

A user interface was implemented in Matlab/Simulink that allowed the user to choose the optimized airfoils shape from a database stored on the computer hard disk and provided to the controller the vertical needed displacements to obtain the desired optimized airfoil shape. The controller activated the power supplies with the needed SMA current values through an analog signal as shown in Fig. 3. In practice, the SMA wires were heated at an approximate temperature of 90°C with a current of 10 A. When the actuator reached the desired position the current was shut off and the SMA was cycled in endless heating/cooling cycles through the controller switching command on/off of the current to maintain the current position until another desired position or the entire system shut-off was required.

In support of the discrete pressure instrumentation, infrared thermography (IR) visualization was performed to detect the transition location on the morphing wing upper surface and validate the pressure sensor analysis. The transition detection method using IR was based on the differences in the laminar and turbulent convective heat transfer coefficient and was exacerbated by the artificial increase of model airflow temperature differences. In the resulting images, the sharp temperature gradient separating high-temperature (white intensity in image) and low-temperature (dark intensity) regions was an indication of the transition location. The infrared camera used was an Agema SC3000 camera, equipped with a 240×320 pixels quantum well infrared photo detector, operating in the infrared wavelength region of 8–9 μm and cooled to 70°K to reduce thermal noise. The camera provided a resolution of 0.02°C and a maximum frame rate of 60 Hz. It was equipped with the default lens (FOV $= 20° \times 15°$), and was installed 1.5 m away from the model with an optical axis oriented in the horizontal plane at about 30 deg with respect to the wing surface midchord normal. Optical access was provided through an opening on the side wall of the test section opposite to the upper surface. More details about the methodology and processing are available in [49].

B. Aerodynamic Detection System and Graphical User Interface

The morphing wing goal was the improvement of the laminar flow over the upper surface of the wing. To ensure that the improvement was real, we built a detection system that gave information about the flow characteristics. An array of 12 Kulite pressure sensors was installed on the flexible skin.

The pressure data acquisition was performed using a NI-DAQ USB 6210 card with 16 analog inputs, at a total sampling rate of 250 kilosamples/s. The input channels were connected directly to

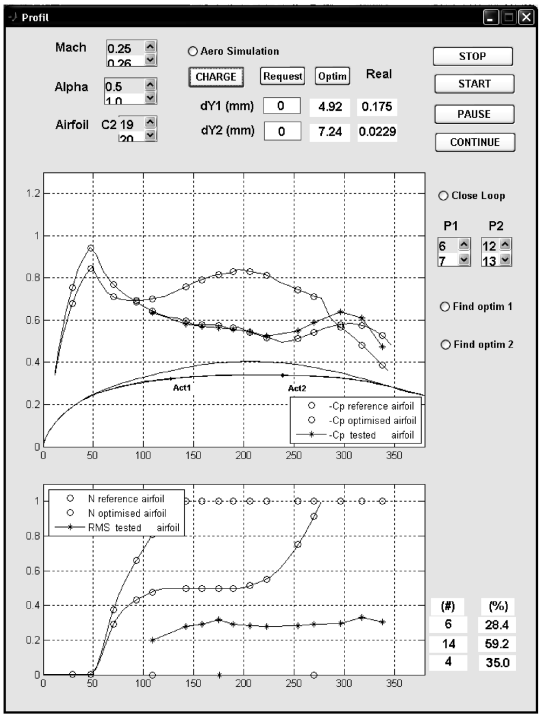

a) Un-morphed configuration

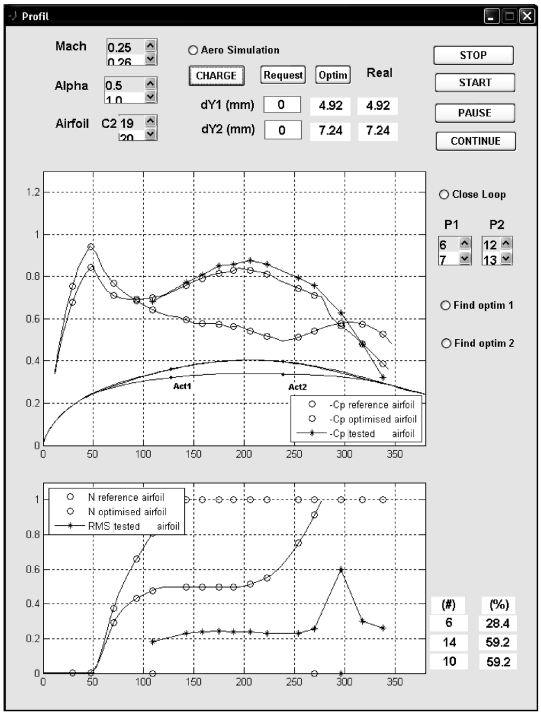

b) Morphed configuration

Fig. 4 GUI with the control buttons of the software.

the IAR-NRC analog data acquisition system, which was connected to the 12 Kulite sensors. The IAR-NRC served as an amplifier and conditioner of the signal at a sampling rate of 15 kilosamples/s. One extra channel was used for the wind-tunnel dynamic pressure acquisition to calculate the pressure coefficients C_ps from the pressure values measured by the 12 pressure sensors. The signal was acquisitioned at a sampling rate of 10 kilosamples/s in frames of 1024 points for each channel, which allowed a boundary-layer pressure fluctuation fast Fourier transform spectral decomposition up to 5 kHz for all channels, at a rate of 9.77 kilosamples/s using Matlab/Simulink software. The plot results were visualized in real time on the computer screen in dedicated windows (see Fig. 4) at a rate of 1 samples/s. Figure 4 shows an example of a graphical user interface in which all the aerodynamic and morphing shape information was centralized together with the control buttons of the controlling software. The window shows information about the Mach number, the angle of attack, the airfoil shape of the morphing wing, and the two actuators' vertical displacements needed to obtain the desired airfoil shape. The two plots show the pressure coefficients distribution C_ps of the 12 Kulite sensors, and the noise of the signal (rms) of each pressure signal. Figure 4a shows the wing unmorphed position, and Fig. 4b shows the wing under its morphed position. The results obtained are qualitatively very similar to those obtained in previous studies [50,51].

The transition between laminar and turbulent flow was detected by means of each pressure signal's rms. The lower rms plot given in Fig. 4 shows the normalized quantity of the pressure signal noise from each Kulite sensor (star points curve). In the example shown in Fig. 4, the rms plot in the unmorphed configuration (Fig. 4a), the transition is shown in the fourth sensor due to the fact that it had the maximum rms value.

In Fig. 4a on the graphical user interface (GUI) an unmorphed airfoil is shown by use of a black color. The actuators' reference positions correspond to $dY1 = 0$ mm and $dY2 = 0$ mm, the C_p distribution calculated by XFoil for the reference airfoil (black curve), and the C_p theoretical values of the sensors shown as black circles on the C_p distribution curve.

In the lower plot of Fig. 4a the N factor used by XFoil to predict transition for the reference airfoil (black curve) is shown. The critical value $N_{\text{cr}} = 7.34$ was used in the simulation to match the turbulence level $T = 0.14\%$ measured in the wind tunnel using Mack's correlation Eq. (1), and the plotted values on the figure are normalized (N/N_{cr}) [52]

$$N_{\text{cr}} = -8.43 - 2.4 \cdot \log(T) \tag{1}$$

In the case of an unmorphed configuration, the predicted transition position was found to be the 6th position of the 16 available sensors' positions. In the beginning of the wind-tunnel tests 16 sensors were installed, but due to their removal and reinstallation during the next two wind-tunnel tests, four of them were found to be defective. Therefore, 12 sensors remained to be used during the last third wind-tunnel tests so that only 12 Kulite sensors were used for plotting the C_p distribution and rms distribution (star plots).

Results predicted for the morphed airfoil are shown in blue color. The morphed airfoil coordinates are shown as blue curves in the upper part of Fig. 4b, the C_p distribution was calculated by XFoil for the optimized airfoil (blue curve), and the C_p theoretical values of the sensors are shown as blue circles on the C_p distribution curve. In the lower plot of Fig. 4b, the N factor used by XFoil to predict transition

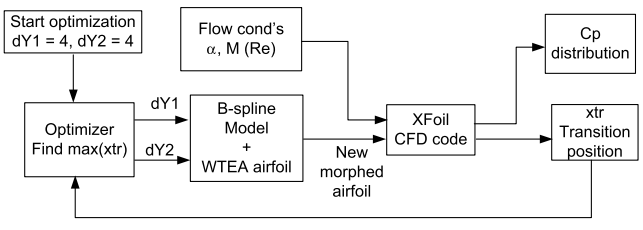

Fig. 5 Optimization logic schematic.

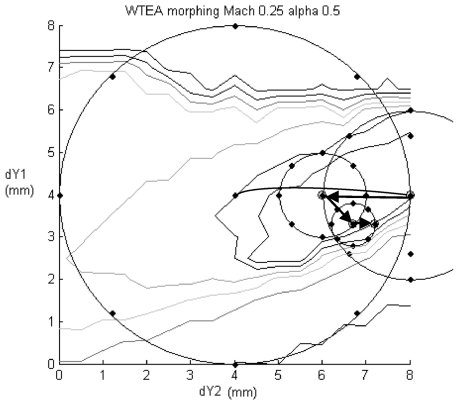

a)

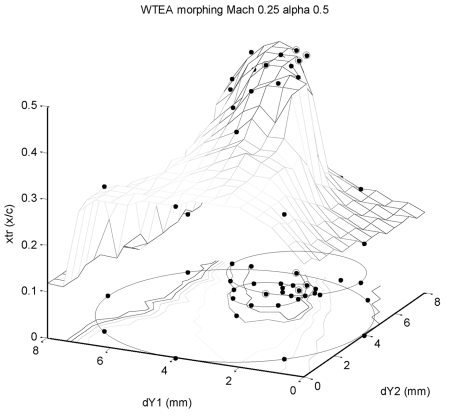

b)

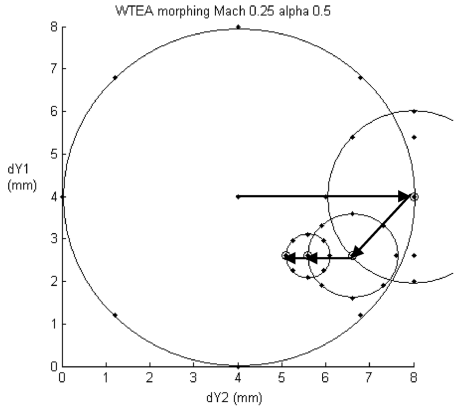

c)

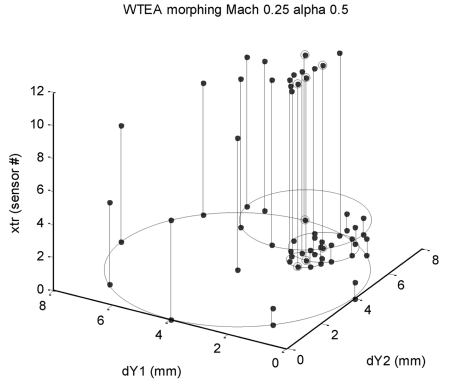

d)

Fig. 6 Optimization in simulation using XFoil code (parts a and b) vs optimization in real time during wind-tunnel tests (parts c and d) for the same airflow conditions $M = 0.25$ and $\alpha = 0.5$ deg.

is shown for the optimized airfoil (blue curve). In this case of morphed configuration, the predicted position of transition was the 14th position of the 16 available sensors' positions.

These black (unmorphed) and blue (morphed) curves served as theoretical validations of the measured value curves reflecting the aerodynamic parameters (C_p and rms) provided by Kulite sensors in real time with a sampling rate of 1 S/s. In Fig. 4b the actuated airfoil in the morphed position ($dY1 = 4.92$ mm and $dY2 = 7.24$ mm) is shown. The transition position was given by the sensor location where the maximum rms was found, which in this case is the 10th Kulite sensor out of 12 sensors. The instant visualization allows us to find the exact position predicted by XFoil.

III. Simulation and Experimental Results Obtained in the Wind Tunnel

The simulation of the system used the Matlab/Simulink software as a programming platform. The simulation used the optimization subroutine exactly the same as in bench tests and wind-tunnel tests, except that in computer simulation and bench tests the aerodynamic pressures that acted upon the skin and stimulated the sensors were simulated by use of XFoil software. A mathematical model of the flexible skin used a *B*-spline with four flexion points. Two points were fixed where the skin was glued on the wing rigid structure and two points were mobile and were placed in the actuators' coordinates on the wing structure. The *B*-spline shape that defines the airfoil's flexible skin did not have the same coordinates as the flexible skin, but was a good approximation for the purpose of designing an optimization subroutine in closed loop with a CFD code. Laser scanning during bench tests showed that the differences between the scanned airfoils and the theoretical airfoils were less than 0.5 mm (less than 6.25% of the maximum actuators' deflection of 8 mm) [53]. The optimization initialized the algorithm with the values $dY1 =$ 4 mm and $dY2 = 4$ mm. Afterward, the algorithm evaluated the transition point position in eight points of coordinates $(dY1, dY2)$ situated on a circle centered on the initial point with a radius of 4 mm within the search domain defined by the bidimensional space of actuators strokes $\{dY1 = [0, 8], dY2 = [0, 8]\}$. For each evaluation point, the x_{tr} value was evaluated by use of XFoil and stored in the memory. After the first round of evaluations the optimizer decided which evaluating point had the maximum value of x_{tr}, which became the initial point for the next round of evaluations. The logic schematic of the optimization subroutine is shown in Fig. 5.

Figures 6a, 6b, and 7 show the result of WTEA airfoil optimization after four evaluation rounds, first evaluation with a radius of 4 mm, second evaluation with a radius of 2 mm, third evaluation with a radius of 1 mm, and fourth and last evaluation with a radius of 0.5 mm. As seen in Fig. 6b, the last round of evaluation was almost unnecessary because the maximum x_{tr} was found inside a plateau of maximums with very small differences between them. Before doing the optimization a mapping of the search domain was performed, that is, for each combination of $dY1$ and $dY2$ in the interval (0 mm, 8 mm) with a step of 1 mm it was found the x_{tr} and was built the surface $x_{\text{tr}} = f(dY1, dY2)$ for the purpose of visualizing the form of the hill. Figures 6c and 6d show the same optimization routine that ran during the wind-tunnel tests in the same airflow conditions as the ones simulated except that there was no map of the searched function. The result was slightly different because the airfoil shape of the real flexible skin under wind-tunnel conditions was different than the airfoil shapes defined by use of *B*-splines. Still, the result was similar in terms of actuator strokes $dY1$ and $dY2$ as well as the position of transition. Similarly, there could be observed in Fig. 6d a plateau of evaluation points that had the transition occurrence on the 11th sensor.

Figure 7 shows the result of the airfoil shape optimization, C_p distribution, and x_{tr} transition point position on the upper surface of the airfoil obtained through simulation using XFoil and a *B*-splines model for the flexible skin. The values obtained for wind flow conditions of Mach $= 0.25$ and $a = 0.5$ are $dY1 = 3.3$ mm and $dY2 = 7.2$ mm. Also in Fig. 7 the *N* factor distribution is shown, which was the parameter used by XFoil to calculate the transition

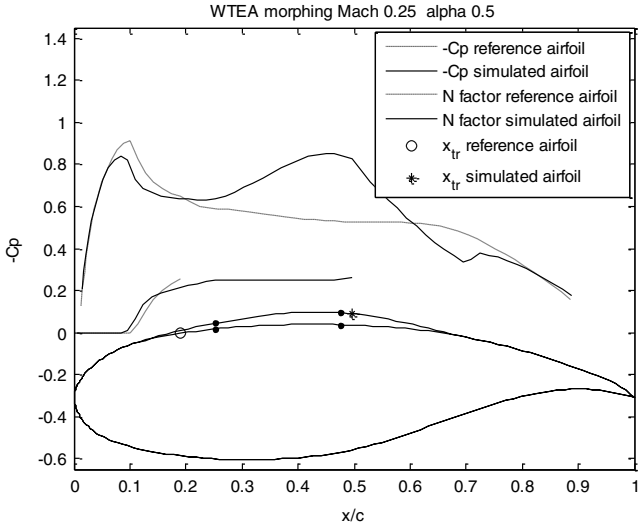

Fig. 7 Optimization simulation results for $M = 0.25$ and $\alpha = 0.5$ deg.

point position. When *N* factor reached the N_{cr} critical value the transition was triggered. This parameter was used in the wind tunnel to validate the transition position found through the rms measuring of the Kulite pressure sensors.

Figure 8 shows the optimized airfoil shape, C_p distribution, and x_{tr} transition point position on the upper surface of the airfoil in wind-tunnel test (red plots) compared with the optimal airfoil plots (blue) and reference airfoil plots (black) obtained through simulation. Also in the lower subplot of Fig. 8, the *N* factor used by XFoil to detect the transition position was compared with the rms of the Kulite sensors. Both the *N* factor and rms were normalized and the purpose of the plots was to have a visual indicator of the transition position.

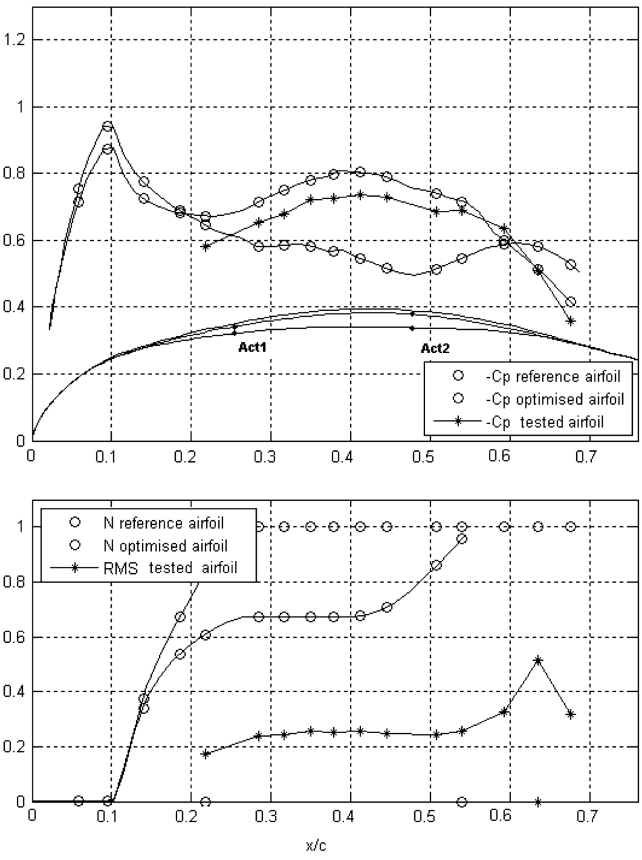

Fig. 8 Optimization result during wind-tunnel test for $M = 0.25$ and $\alpha = 0.5$ deg.

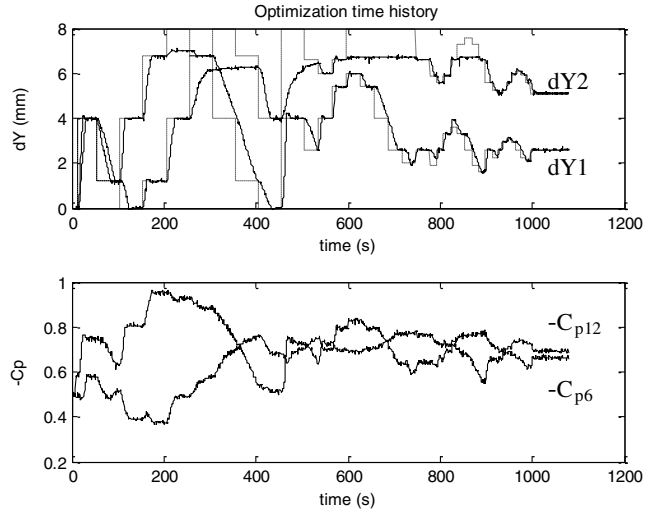

Fig. 9 Optimization time history during wind-tunnel test for $M = 0.25$ and $\alpha = 0.5$ deg.

The software considered the transition position in the coordinates of the sensor with the highest noise (rms) as confirmed by previous studies [50]. The values obtained in the wind tunnel for wind flow conditions of Mach $= 0.25$ and $a = 0.5$ are $x_{\text{tr}}/c = 0.635$ ($x_{\text{tr}} = 317.5$ mm) for the actuator displacement values $dY1 = 2.6$ mm and $dY2 = 5.1$ mm.

Figure 9 shows the time history of the optimization process in the wind-tunnel. Because of the long response of the SMA actuators (the time of cooling from maximum displacement to zero was approx 2 min), the entire process of optimum search converged to the optimum values in approximately 20 min. Also, it can be observed that the requested displacements of the actuators at the maximum displacement of 8 mm were not realized, due to the fatigue of the SMAs accumulated in previous testes. The maximum deflection was in fact 7 mm for the first actuator and 6.5 mm for second actuator.

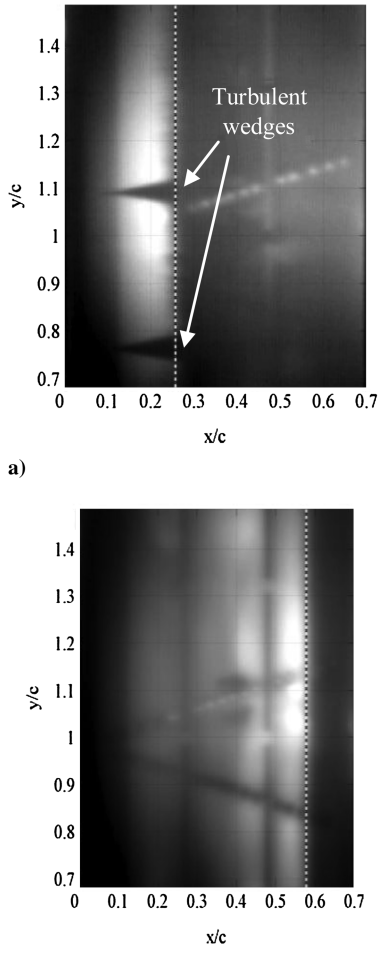

Fig. 10 Infrared results obtained at $M = 0.25$ and $\alpha = 0.5$ deg in a) reference, and b) after optimization.

Figure 10 shows typical infrared results obtained at $M = 0.25$, $\alpha = 0.5$ deg for various configurations. Only the composite portion of the wing at $x/c \leq 0.7$ was shown. The white spots on the wing are the electronically heated Kulite pressure transducers. The two lines of SMA actuators, colder than the model surface, were also visible at quarter chord and near midchord. The locations of the transition in the images have been highlighted using a white dashed line; it corresponds to the location of a large surface temperature gradient, the laminar region being about 2–3°C hotter than the turbulent region. The reference airfoil configuration (Fig. 10a) showed a transition location at $x/c = 26\%$. The optimization (Fig. 10b) allowed a laminar boundary-layer run to $x/c = 58\%$, which represented a significant improvement over the reference case (Fig. 10a). Some turbulent wedges caused by leading-edge contamination due to dust particles in the flow were visible in Fig. 10a. In addition to providing an online verification of the Kulite dynamic pressure signals, the infrared measurement was particularly useful to detect those early artificial turbulent regions. When the level of contamination was estimated unacceptable or likely to affect the drag or the Kulite measurements, the test was interrupted and the model was carefully cleaned.

IV. Conclusions

The results of the tests performed in a wind tunnel using a morphing wing were shown. The optimization method did not use any CFD code but used the same optimization algorithm in real time. This optimization converged in approximately 10 min due to the slow response of the SMA actuators, especially in the cooling phase of the cycle. It was observed that the airfoil realized by this method slightly differs from the optimization using CFD codes. This result was due to the fact that the cost function of the optimization (transition position) had discrete values (the sensor's positions) and the maximum of the function was a plateau of different $dY1$ and $dY2$ values. The optimizer stopped at a certain value in function of the number and magnitudes of the searching steps. It was observed that the last searching step (searching of the maximum in eight points situated on a circle with ray of 0.5 mm, see Fig. 6) was not necessary due to the cost function plateau of maximums.

Acknowledgments

The authors would like to thank the Consortium of Research in the Aerospatial Industry in Quebec for funding the present work, and Thales Avionics and Bombardier Aerospace for their financial and technical. The authors would like also to thank George Henri Simon for initiating the Consortium of Research in the Aerospatial Industry in Quebec 7.1 project and Philippe Molaret from Thales Avionics for their collaboration on this work.

References

[1] Zingg, D. W., Diosady, L., and Billing, L., "Adaptive Airfoils for Drag Reduction at Transonic Speeds," AIAA Paper 2006-3656, 2006.

[2] Munday, D., and Jacob, J., "Active Control of Separation on a Wing With Conformal Camber," AIAA Paper 2001-0293, 1998.

[3] Jacob, J. D., "Aerodynamic Flow Control Using Shape Adaptive Surfaces," *ASME 17th Biennial Conference on Mechanical Vibration and Noise, Symposium on Structronics, Mechatronics, and Smart Materials*, American Society of Mechanical Engineers Paper No. DETC99/VIB-8323, Sept. 1999, http://www.engr.uky.edu/~fml/papers/VIB-8323.pdf [retrieved 6 Nov. 2009].

[4] Munday, D., and Jacob, J., "Low Speed Morphing Wing Flow Control," Univ. of Kentucky, Lexington, KY, 2001, http://www.engr.uky.edu/~fml/research/wing-2001.pdf [retrieved 6 Nov. 2009].

[5] Munday, D., Jacob, J. D., and Huang, G., "Active Flow Control of

Separation on a Wing with Oscillatory Camber," *40th AIAA Aerospace Sciences Meeting*, AIAA Paper No. 2002-0413, 2002.

[6] Munday, D., Jacob, J. D., Hauser, T., and Huang, G., "Experimental and Numerical Investigation of Aerodynamic Flow Control Using Oscillating Adaptive Surfaces," *1st AIAA Flow Control Conference*, AIAA Paper No. 2002-2837, 2002, http://www.engr.uky.edu/~fml/papers/AIAA-2002-2837.pdf [retrieved 6 Nov. 2009].

[7] Jacob, J. D., "On the Fluid Dynamics of Adaptive Airfoils," Univ. of Kentucky, Lexington, KY, http://www.engr.uky.edu/~fml/papers/imece-paper.pdf [retrieved 6 Nov. 2009].

[8] Lutz, T., Sommerer, A., and Wagner, S., "Design Of Adaptive Transonic Airfoils By Means Of Numerical Optimisation," Univ. of Stuttgart, Stuttgart, Germany, 2000.

[9] Wadehn, W., Sommerer, A., Lutz, T., Fokin, D., Pritschow, G., and Wagner, S., "Structural Concepts and Aerodynamic Design of Shock Control Bumps," *Proceedings 23nd ICAS Congress*, International Council of the Aeronautical Sciences Paper 66R1.1, Toronto, 2002.

[10] Sobieczky, H., and Geissler, W., "Active Flow Control Based On Transonic Design Concepts," *DLR German Aerospace Research Establishment*, AIAA Paper 99-3127, 1999.

[11] Sobieczky, H., Geissler, W., and Hannemann, M., "Expansion Shoulder Bump for Wing Section Viscous/Wave Drag Control," *FLOWCON IUTAM Symposium on Mechanics of Passive and Active Flow Control*, Gottingen, Germany, 1998.

[12] Martins, A. L., and Catalano, F. M., "Aerodynamic Optimization Study of a Mission Adaptive Wing for Transport Aircraft," International Council of the Aeronautical Sciences Paper 96, Sorrento, Italy, 1996.

[13] Martins, A. L., and Catalano, F. M., "Viscous Drag Optimization for a Transport Aircraft Mission Adaptive Wing," International Council of the Aeronautical Sciences Paper 98-31499, Melbourne, Australia, 1998.

[14] Catalano, F. M., Greco, P. C., and Martins, A. L., "Viscous And Wave Drag Optimization For a Transport Aircraft Mission Adaptive Wing," *Aircraft Laboratory: University of São Paulo-Brazil and EMBRAER, Congress*, International Council of the Aeronautical Sciences, Toronto, 2002.

[15] Martins, A. L., and Catalano, F. M., "Drag Optimisation For Transport Aircraft Mission Adaptive Wing," *Journal of the Brazilian Society of Mechanical Sciences*, Vol. 25, No. 1, 2003.

[16] Arcara, P. C. Jr., Bartlett, D. W., and McCullers, L. A., "Analysis for the Application of Hybrid Laminar Flow Control to a Long-Range Subsonic Transport Aircraft, *Aerospace Technology Conference and Exposition*, Society of Automotive Engineers Paper 912113, Warrendale, PA, 1991, pp. 1–15.

[17] Allison, D. O., and Dagenhart, J. R., "Design of a Laminar-Flow-Control Supercritical Airfoil for a Swept Wing," *CTOL Transport Technology*, NASA Langley Research Center, Hampton, VA, 1978, pp. 395–408.

[18] Hackenberg, and Petra, "Numerical Optimization of the Suction Distribution for Laminar Flow Control Aerofoils," Doctoral Thesis, Univ. of Southampton, Southampton, England, 1995.

[19] Pralits, J., "Optimal Design of Natural and Hybrid Laminar Flow Control on Wings," Doctoral Thesis, Royal Institute of Technology, Stockholm, Sweden, 2003.

[20] Rioual, J.-L., Nelson, P. A., and Fisher, M. J., "Experiments on the Automatic Control of Boundary-Layer Transition," *Journal of Aircraft*. Vol. 31, No. 6, 1994, pp. 1416–1418. doi:10.2514/3.46668

[21] Manzo, J., Garcia, E., and Wickenheiser, A. M., "Adaptive Structural Systems and Compliant Skin Technology of Morphing Aircraft Structures," *Proceedings of SPIE: The International Society for Optical Engineering*, Vol. 5390, 2004, pp. 225–234.

[22] Namgoong, H., Crossley, W. A., and Lyrintzis, A. S., "Morphing Airfoil Design for Minimum Aerodynamic Drag and Actuation Energy Including Aerodynamic Work," AIAA Paper 2006-2041, 2006, pp. 5407–5421.

[23] Barrett, R., "Improvements to Commercial and General Aviation Via Adaptive Aerostructures," *7th AIAA Aviation Technology, Integration and Operations Conference (ATIO)*, AIAA Paper 2007-7873, Sept. 2007, pp. 1–9.

[24] Gandhi, N., Jha, A., Monaco, J., Siegler, T. M., Ward, D., and Inman, D. J., "Intelligent Control of a Morphing Aircraft, AIAA Paper 2007-1716, 2007, pp. 166–182.

[25] Skillen, M. D., and Crossley, W. A., "Developing Response Surface Based Wing Weight Equations for Conceptual Morphing Aircraft Sizing," AIAA Paper 2005-1960, 2005, pp. 2007–2019.

[26] Scherer, L. B., West, M., Florance, J. P.., Wieseman, C. D., Burner, A. W., and Fleming, G. A., "DARPA/AFRL/NASA Smart Wing Second Wind Tunnel Test Results," 1999, http://www.tpub.com/content/nasa1999/NASA-99-6spie-lbs/index.htm [retrieved 6 Nov. 2009].

[27] Yang, S.-M., Han, J. H., and Lee, I., "Characteristics of Smart Composite Wing with SMAs and Optical Fibre Sensors," *International Journal of Applied Electromagnetics and Mechanics*, Vol. 23, 2006, pp. 177–186.

[28] Bharti, S., "Optimal Structural Design of a Morphing Aircraft Wing Using Parallel Non-Dominated Sorting Genetic Algorithm Ii (Nsga Ii)," *Smart Structures and Materials 2006: Industrial and Commercial Applications of Smart Structures Technologies*, edited by D. K. Lindner, Vol. 6166, Proceedings of SPIE: The International Society for Optical Engineering, 2006, pp. 1–12.

[29] Ricci, S., and Terraneo, M., "Application of MDO Techniques to the Preliminary Design of Morphed Aircraft," AIAA Paper 2006-7018, 2006, pp. 1263–1276.

[30] Sanders, B., "Aerodynamic and Aeroelastic Characteristics of Wings with Conformal Control Surfaces for Morphing Aircraft," *Journal of Aircraft*, Vol. 40, No. 1, 2003, pp. 94–99. doi:10.2514/2.3062

[31] Love, M. H., "Impact of Actuation Concepts on Morphing Aircraft Structures," AIAA Paper 2004-1724, 2004, pp. 2355–2366.

[32] Bye, D. R., and McClure, P. D., "Design of a Morphing Vehicle," AIAA Paper 2007-1728, 2007, pp. 321–336.

[33] Koma, A. Y., and Zimcik, D. G., "Applications of Smart Structures to Aircraft for Performance Enhancement," *Canadian Aeronautics and Space Journal*, Vol. 49, No. 4, 2003.

[34] Flanagan, J. S., Strutzenberg, R. C., Myers, R. B., and Rodrian, J. E., "Development and Flight Testing of a Morphing Aircraft, the Nextgen Mfx-1," AIAA Paper 2007-1707, 2007, pp. 73–75.

[35] Andersen, G. R., Cowan, D. L., and Piatak, D. J., "Aeroelastic Modeling, Analysis and Testing of a Morphing Wing Structure," AIAA Paper 2007-1734, 2007, pp. 359–373.

[36] Ataei-Esfahani, A., and Wang, Q., "Robust Failure Compensation for a Morphing Aircraft Model Using a Probabilistic Approach," *IEEE Transactions on Control Systems Technology*, Vol. 15, No. 2, March 2007, pp. 324–331. doi:10.1109/TCST.2006.883188

[37] Kroo, I., Prinz, F., and Eaton, J., "UAV Aero-Elastic Control Using Redundant Micro-Actuators," Rept. A641214, 1999.

[38] De Breuker, R., Abdalla, M., Gurdal, Z., and Lindner, D., "Energy-Based Aeroelastic Analysis of a Morphing Wing," *Proceedings of SPIE: The International Society for Optical Engineering*, Vol. 6523, No. , 2007, pp. 1–12.

[39] Neal, D. A., Farmer, J., and Inman, D., "Development of a Morphing Aircraft Model for Wind Tunnel Experimentation," AIAA Paper 2006-2141, 2006, pp. 6443–6456.

[40] Smith, K., Butt, J., von Spakovsky, M. R., and Moorhouse, D., "A Study of the Benefits of Using Morphing Wing Technology in Fighter Aircraft Systems," AIAA Paper 2007-4616, 2007, pp. 1497–1508.

[41] Love, M. H., Zink, P., Stroud, R., Bye, D., Rizk, S., and White, D., "Demonstration of Morphing Technology Through Ground and Wind Tunnel Tests," AIAA Paper 2007-1729, 2007, pp. 337–348.

[42] Popov, A.-V., Labib, M., Fays, J., and Botez, R. M., "Closed Loop Control Simulations on a Morphing Laminar Airfoil Using Shape Memory Alloys Actuators," *Journal of Aircraft*, Vol. 45, No. 5, 2008, pp. 1794–1803. doi:10.2514/1.37073

[43] Coutu, D., Brailovski, V., and Terriault, P., "Promising Benefits of an Active-Extrados Morphing Laminar Wing," *Journal of Aircraft*, Vol. 46, No. 2, 2009, pp. 730–731. doi:10.2514/1.40657

[44] Georges, T., Brailovski, V., Morellon, E., Coutu, D., and Terriault, P., "Design of Shape Memory Alloy Actuators for Morphing Laminar Wing With Flexible Extrados," *Journal of Mechanical Design*, Vol. 131, No. 9, 2009, pp. 091006-1–091006-9.

[45] Sainmont, C., Paraschivoiu, I., and Coutu, D., "Multidisciplinary Approach for the Optimization of a Laminar Airfoil Equipped with a Morphing Upper Surface," NATO Paper AVT-168, Evora, Portugal, 2009.

[46] Khalid, M., "Navier–Stokes Investigation of Blunt Trailing Edge Airfoils Using O-Grids," *Journal of Aircraft*, Vol. 30, No. 5, 1993, pp. 797–800. doi:10.2514/3.46416

[47] Khalid, M., and Jones, D. J., "A CFD Investigation of the Blunt Trailing Edge Airfoils in Transonic Flow," *Inaugural Conference of the CFD Society of Canada*, CFD Society of Canada, Montreal, June, 1993.

[48] Popov, A.-V., Botez, R. M., and Grigorie, L., "Morphing Wing Validation during Bench Tests," *2009 Canadian Aeronautics and Space Institute Annual General Meeting, Aircraft Design & Development*

Symposium, Kanata, Ontario, 2009.

[49] Mébarki, Y., Mamou, M., and Genest, M., "Infrared Measurements of Transition Location on the CRIAQ project Morphing Wing Model," Nuclear Regulatory Commission Paper LTR- AL-2009-0075, 2009.

[50] Nitcshe, W., Mirow, P., and Dorfler, T., "Investigations on Flow Instabilities on Airfoils by Means of Piezofoil: Arrays," *Laminar-Turbulent Transition IUTAM Symposium*, Springer–Verlag, New York, 1989.

[51] Mangalam, S. M., "Real-Time Extraction of Hydrodynamic Flow Characteristics Using Surface Signature," *IEEE Journal of Oceanic Engineering*, Vol. 29, No. 3, July 2004, pp. 622–630. doi:10.1109/JOE.2004.833098

[52] Mack, L. M., "Transition and Laminar Instability," Jet Propulsion Laboratory Publication Paper 77-15, Pasadena, CA, 1977.

[53] Popov, A. V., Grigorie, L. T., and Botez, R. M., "Control of a Morphing Wing in Bench Test," *13th Canadian Aeronautical and Aerospace Institute CASI Aeronautics Conference*, Kanata, Ontario, 5–7 May, 2009.